

Line spectroscopy with spatial resolution of laser–plasma X-ray emission

L. LABATE,^{1,2} M. GALIMBERTI,^{1,2} A. GIULIETTI,¹ D. GIULIETTI,^{1,2} L.A. GIZZI,¹
R. NUMICO,¹ AND A. SALVETTI,¹

¹Intense Laser Irradiation Laboratory—IFAM, Area della Ricerca—CNR, Pisa, Italy

²Dipartimento di Fisica, Università di Pisa and INFN, Pisa, Italy

(RECEIVED 24 January 2001; ACCEPTED 5 February 2001)

Abstract

High dynamic range, space-resolved X-ray spectra of an aluminum laser–plasma in the 5.5–8 Å range were obtained using a TiAP crystal and a cooled CCD camera as a detector. This technique was used to investigate the emission region in the longitudinal direction over a distance of approximately 350 μm from the solid target surface. These data show that the electron density profile varies by two orders of magnitude with the temperature ranging from about 180 eV in the overdense region to about 650 eV in the underdense region. Accordingly, different equilibria take place across the explored region which can be identified with this experimental technique. Detailed studies on highly ionized atomic species in different plasma conditions can therefore be performed simultaneously under controlled conditions.

1. INTRODUCTION

Plasmas generated by high-power, nanosecond laser irradiation of solid targets exhibit a wide range of physical conditions due to the large variation of electron density and temperature both in space and time. In the coronal region, where coupling mechanisms between the laser light and the plasma mostly take place, the atomic physics is dominated by radiative processes, and the so-called coronal equilibrium provides a good description of the system independent of the specific structure of energy levels in the plasma. As we go towards the regions of higher electron density, collisions start to contribute and a simple description is no longer possible: A detailed analysis must be performed which takes into account atomic properties as well as statistical quantities. This so-called collisional-radiative equilibrium can be treated numerically and only for a given set of energy levels. In the densest part of laser plasmas, collisions may dominate and local thermodynamic equilibrium may provide again a simple description. On the other hand, once the particular equilibrium is known, X-ray emission can be exploited as a powerful diagnostic tool for characterization of laser-plasmas (Giulietti & Gizzi, 1998). This is particularly true in the case of very dense plasmas, which cannot be easily studied by

other diagnostic techniques like interferometric methods (Kauffman, 1991; Griem, 1997).

X-ray spectroscopy with spatial resolution allows the plasma parameters like electron temperature, density, or ionization state to be measured at different regions. Laser-plasma interaction processes including nonlinear interaction phenomena in the underdense region, such as filamentation or self-focusing, two-plasmon decay instability or any other mechanism which affects the electron distribution function significantly, can be studied by X-ray spectroscopy with spatial resolution. Further, spatially resolved spectra can be used to study strongly correlated plasmas of high density (Leboucher-Dalimier *et al.*, 1993) or the gain region for X-ray lasers (Nantel *et al.*, 1996). Finally, the knowledge of spatial characteristics of laser-produced plasmas allows X-ray sources for applications to be optimized (see Giulietti *et al.*, 1998; Marzi *et al.*, 2000, and references therein).

The main obstacle to an extensive use of this technique is that a micron-scale resolution requires a very narrow slit, with a consequent dramatic reduction of the X-ray flux. For this reason, this class of experiments has been limited in the past to relatively low resolution (large slits) and low spectral dispersion. The recent availability of high dynamic range CCD X-ray detectors now makes it possible to perform these studies at an unprecedented spatial/spectral resolution, with the possibility of reaching the micron resolution level (X-ray spectromicroscopy). In this report, we describe our experimental technique to obtain space-resolved spectra

Address correspondence and reprint requests to: Luca Labate, Istituto di Fisica Atomica e Molecolare, CNR, Area della ricerca, Via Moruzzi, 1-56124, Pisa, Italy. E-mail: luca@ifam.pi.cnr.it

of laser-produced plasmas and we show that the combination of a back-illuminated CCD detector and a flat crystal result in a high-sensitivity instrument well suited for high spatial/spectral resolution studies of small (10–1000 μm) X-ray sources.

2. EXPERIMENTAL SETUP

The experimental setup inside the interaction chamber is shown in Figure 1. The plasma was produced by focusing a Nd:YLF laser beam ($\lambda = 1.053 \mu\text{m}$) with an $f/4$ lens onto a rotating cylindrical Al target. The laser, a transversally and longitudinally monomode system, provided an energy up to 3 J in each 3-ns (FWHM) Gaussian pulse. Shot-to-shot fluctuations in the total energy delivered on the target were limited to 10%. The laser beam had a Gaussian spatial distribution which resulted in a focal spot size of about 6 μm (FWHM) with a Rayleigh length of about 100 μm , resulting in an intensity on the target up to $5 \times 10^{14} \text{ W/cm}^2$.

A flat *thallium hydrogen phthalate* (TIAP) crystal ($2d = 25.9 \text{ \AA}$) coupled to a back-illuminated Peltier-cooled CCD camera was used to spectrally resolve X-ray emission from the plasma. The crystal, set in a first-order Bragg configuration, and the CCD camera were placed at an angle of 45° with respect to the laser beam axis, that is, 25° from the plasma expansion axis (see Fig. 1).

The spectrometer allowed the spectral region from 5.5 to 8 \AA to be investigated. A typical spatially integrated spectrum in this range, obtained using the setup of Figure 1 but without the use of the slit, is shown in Figure 2. The resonance lines from Al XI (lithium-like), Al XII (helium-like), and Al XIII (hydrogen-like) ions are visible, together with their satellites. Also visible is the intercombination line (IC), which results from the $1s2p \ ^3P \rightarrow 1s^2 \ ^1S$ transition in the Al XII ions. This transition, normally forbidden by the spin selection rule in L - S coupling, becomes allowed due to the

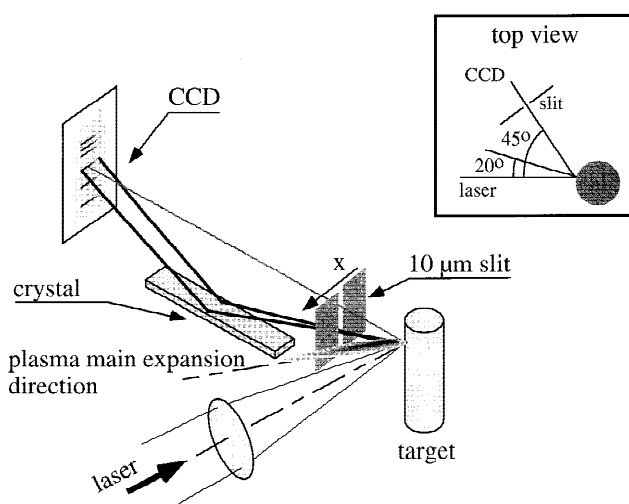


Fig. 1. Schematic setup of the experiment showing the arrangement of the crystal spectrometer and the geometry of the interaction.

mixing of the $1s2p \ ^3P$ and $1s2p \ ^1P$ states in helium-like ions.

Spectral resolution is determined by the size of the emitting region, by the size of the CCD pixels and by the rocking angle of the crystal. Therefore the resolving power is approximately given by (Hauer et al., 1991)

$$\frac{\lambda}{\delta\lambda} = \sqrt{\frac{\tan^2 \vartheta_B}{(\delta\vartheta_c)^2 + (\delta x/L)^2 + (\delta y/L)^2}}, \quad (1)$$

where ϑ_B is the Bragg angle, $\delta\vartheta_c \approx 10^{-4}$ rad is the TIAP rocking angle, $L \approx 20$ cm is the total distance of the source to the CCD, and $\delta x \approx 100 \mu\text{m}$ and $\delta y \approx 24 \mu\text{m}$ are, respectively, the size of the emitting region and of the CCD pixel. Thus, for $\lambda = 7 \text{ \AA}$, we get a resolving power $\lambda/\delta\lambda \approx 5 \times 10^2$, which is dominated by the source size. Notice that the value of 100 μm for the source size is just an order of magnitude; actually, the source size depends on the wavelength considered, as shown in the next section.

The direction perpendicular to the spectral axis in the plane of the CCD matrix can be exploited to spatially resolve the spectrum. To accomplish this task, a 10- μm slit was used (see Fig. 1), which allowed us to obtain spectra with a spatial resolution of about 20 μm along the plasma expansion axis.

3. RESULTS AND DISCUSSION

Figure 3 shows a portion of a typical space-resolved spectrum obtained with the setup of Figure 1. From this spectrum, we can immediately determine the plasma X-ray source longitudinal size, that is, the size along the main plasma expansion direction, corresponding to the normal to the target surface. Figure 4 displays the intensity of the $\text{He}\alpha$ line as a function of the distance from the original target surface (hereafter labelled as z). The spatial resolution is about 20 μm . The size of the emitting region, defined as the FWHM of the $\text{He}\alpha$ intensity profile, is about 280 μm .

To obtain the plasma electron temperature and density profiles, we used the well-known method based on the measurement of the ratio between the intensity of two spectral lines. To this purpose, the comparison of measured line ratios with the predictions of the steady-state atomic physics code RATION (Lee et al., 1984) was performed. The code was set to calculate atomic populations and line intensities assuming collisional-radiative equilibrium (CRE) for a steady-state, homogeneous plasma of a given size, temperature, and density, including opacity effects; a discussion about the applicability of these assumptions to our experimental conditions is given in Macchi et al. (1996). To retrieve the electron temperature and density, however, the plasma transverse dimension along the line of sight has to be considered, to take into account the opacity effects. This information can be obtained from spatially integrated spectra, like the one shown in Figure 2, as we describe in the next subsection.

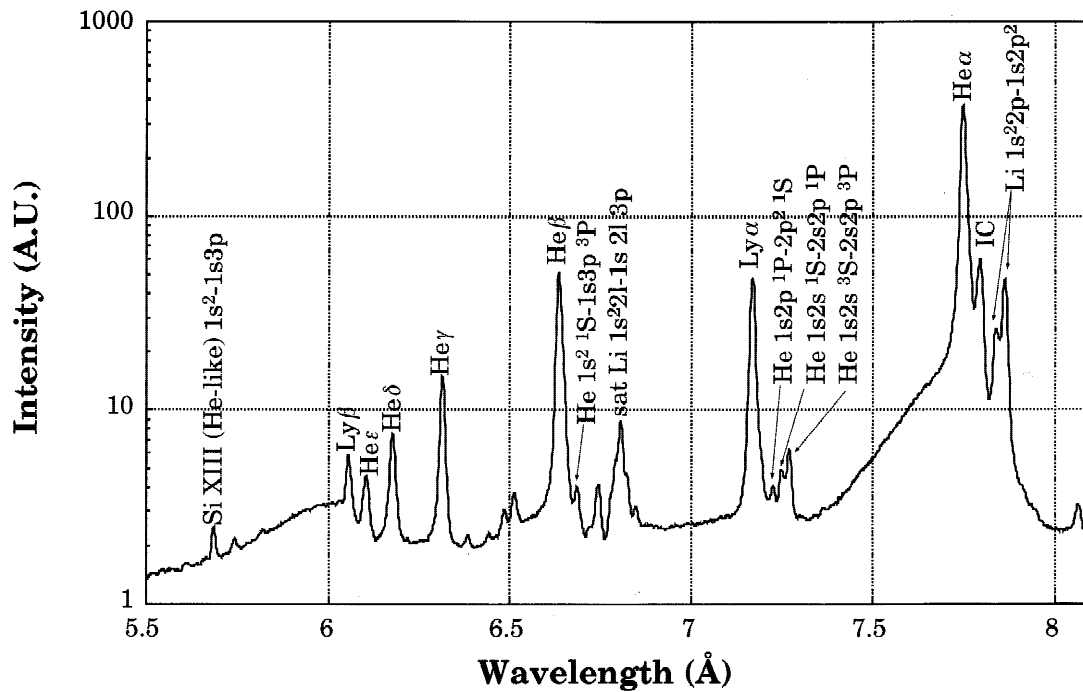


Fig. 2. Spatially integrated spectrum of X-ray radiation in the range from 5.5 to 8 Å emitted by an Al plasma generated from laser irradiation of a solid target.

3.1. Source dimensions and opacity effects

As we have seen above, the source size dominates the spectral resolution $\delta\lambda$, which is much larger than the atomic linewidth, basically due to Doppler and pressure broadening. The size of the emitting region for each spectral line in the direction of the spectral dispersion can then be determined by the instrumental linewidth. Indeed a spatial extension δx of the source induces a broadening $\delta\lambda_o$ of the observed line at wavelength λ given by

$$\delta\lambda_o = \sqrt{\delta\lambda_c^2 + \left(\frac{\delta x}{L \tan \vartheta_B}\right)^2 \lambda^2}, \quad (2)$$

where ϑ_B and L are as in formula (1) and $\delta\lambda_c = \delta\vartheta_c \lambda_B / \tan \vartheta_B$ is the broadening due to the crystal rocking curve. Formula (2) allows the source size δx to be estimated from the linewidths $\delta\lambda_o$ knowing $\delta\lambda_c$ and L .

The geometrical parameter L was retrieved with great precision by studying the pattern of the spectral lines in the plane of the CCD matrix. In fact, a given wavelength λ emitted by a point source and dispersed by the crystal is collected in a curved path resulting from the intersection of the CCD matrix plane with a cone having the vertex in the virtual source position. Position and curvature of these paths obviously depend on the geometrical parameters of the spec-

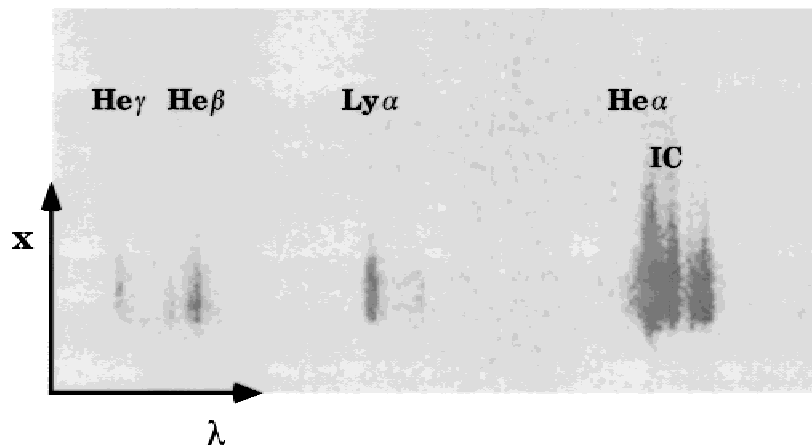


Fig. 3. Spatially resolved spectrum. x refers to the direction indicated in Figure 1.

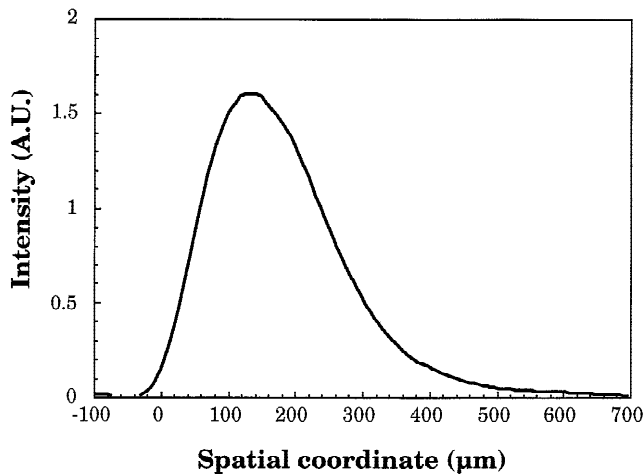


Fig. 4. Measured intensity of the He α line from the plasma as a function of the distance from the target plane (corresponding to “0”). This plot was obtained from the space-resolving spectrograph shown in Figure 1.

rometer, including L , which can thus be retrieved by a careful study of the images obtained by the CCD. The finite extent of the source does not affect this consideration, resulting only in a broadening of the lines.

The size of the emitting region was determined for three different spectral lines, namely He α , He β , and Ly α . Geometrical considerations, together with the assumption of cylindrical symmetry around the main plasma expansion direction, allowed us to get the transverse, that is, normal to the expansion axis, size of the emitting regions. The values obtained are $\delta x = 78 \pm 7 \mu\text{m}$, $\delta x = 66 \pm 5 \mu\text{m}$, $\delta x = 54 \pm 4 \mu\text{m}$ respectively for the He α , He β , and Ly α lines. These results show that the size of the emitting region of the hydrogen-like Ly α line is smaller than the corresponding size for the helium-like lines. This is the first evidence of a strong spatial dependence of the electron temperature which affects the distribution of H-like and He-like ions across the plasma.

3.2. Temperature and density profiles

To obtain a detailed profile of electron temperature and electron density, we measured the spatial behavior of two line intensity ratios, namely Ly α to He β and He α to IC, from the space-resolved spectrum of Figure 3. This last ratio was chosen because of its strong dependence upon the electron density due to the collisional coupling among $1s2p$ states of helium-like ions (Duston & Davis, 1980). Figures 5a and 5b show the spatial behavior of the two line intensity ratios. These data were compared with the predictions of RATION simulations performed assuming different plasma sizes: As an example, Figure 6 displays the Ly α -to-He β intensity ratio as a function of the electron temperature, for different electron densities, obtained assuming a plasma size of $75 \mu\text{m}$.

Comparison of RATION simulations performed for different plasma sizes allowed us to easily estimate the electron

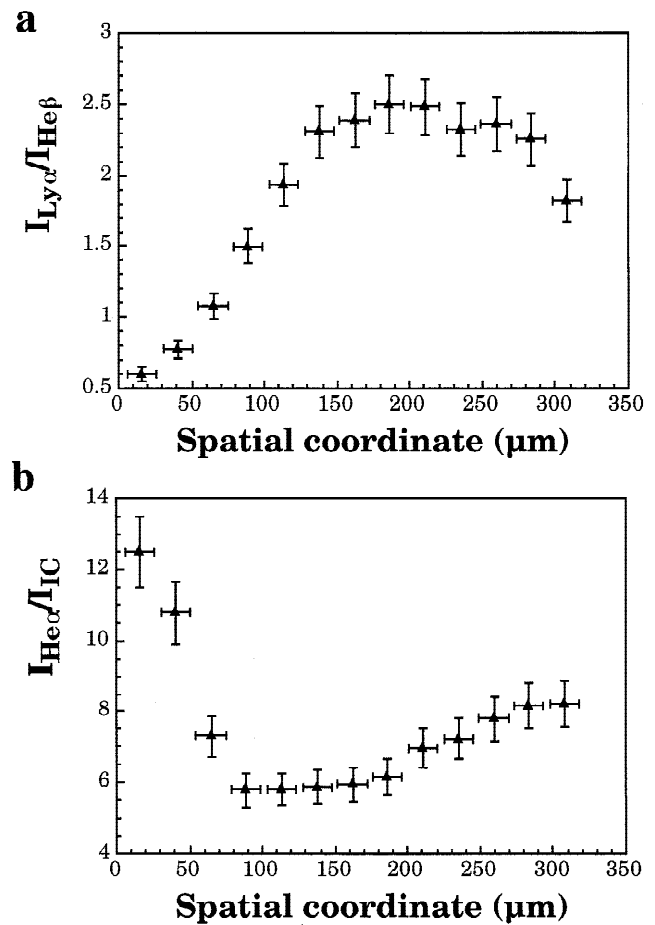


Fig. 5. Measured Ly α to He β (a) and He α to IC (b) intensity ratios as a function of the distance from the original target position along the plasma main expansion direction.

density and temperature at the boundaries of the explored region, namely for $z \lesssim 75 \mu\text{m}$ and for $z \gtrsim 200 \mu\text{m}$. This comparison was simplified by the negligible opacity of the plasma in these regions for the selected transitions in our experimental conditions. In particular, for $z \gtrsim 200 \mu\text{m}$ we obtained a nearly constant temperature of about 650 eV. In contrast, a much lower electron temperature (≈ 180 eV) as well as a density greater than the critical one were estimated for $z \lesssim 75 \mu\text{m}$. Therefore we can expect a strong density and temperature gradients in the intermediate region, although we were not able to obtain detailed profiles. To overcome this difficulty we used the 1D Lagrangian hydrodynamics code MEDUSA to calculate the density profile in this region (Christiansen *et al.*, 1974; Rodgers *et al.*, 1989). The solid curve of Figure 7 shows the density profile calculated by MEDUSA in our interaction conditions. However, we point out here that the use of a 1D simulation to describe our interaction condition results in a serious overestimation of the electron density for distances from the target plane much greater than the plasma transverse dimension (Max, 1982). Previous studies performed by our group showed, in fact, a considerable discrepancy between 1D electron density pro-

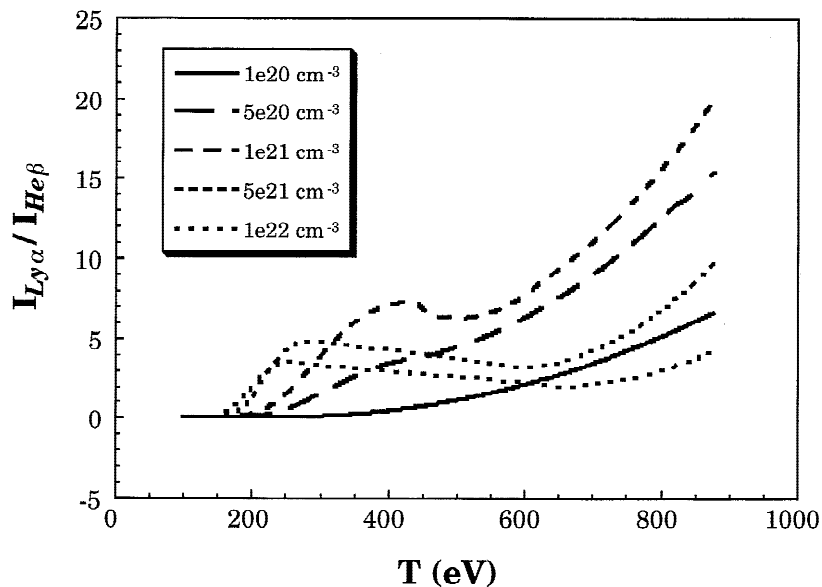


Fig. 6. Calculated Ly α to He β intensity ratio as a function of the electron temperature for a plasma size of 75 μm and for five different electron densities.

file simulation and experimental profiles obtained by interferometric techniques (Gizzi *et al.*, 1994). As shown in Figure 7, in the experimental condition considered in this work, MEDUSA simulations performed in a planar geometry give a nearly constant electron density ($\approx 10^{22} \text{ cm}^{-3}$) over the whole 500- μm range. This result is in clear disagreement with the results obtained for $z \gtrsim 200 \mu\text{m}$, where an electron density of the order of 10^{20} cm^{-3} can be inferred from the comparison with RATION simulations. We have successfully overcome this problem using an option of MEDUSA to run simulations in a 1D spherical interaction geometry, instead of the planar geometry. In fact, we found that such a geometry resulted in a more reliable prediction of electron density profiles than the planar geometry for dis-

tances from the target much greater than the initial plasma transverse dimension size. Here by initial plasma transverse size, we refer to the transverse size at the beginning of the plasma formation process, that is, to the laser focal spot diameter ($\sim 10 \mu\text{m}$). MEDUSA was therefore set to perform hydrodynamic simulations of our experimental conditions by simulating a uniform irradiation of a spherical target. The result is shown in Figure 7 where the density profiles obtained at the peak of the pulse are shown for three different target radii. The simulation corresponding to a target radius of 100 μm provided density values well in agreement with our estimation from spectroscopic measurements in the external regions (for $z \lesssim 75 \mu\text{m}$ and for $z \gtrsim 200 \mu\text{m}$). Therefore we used this electron density profile of the plasma to

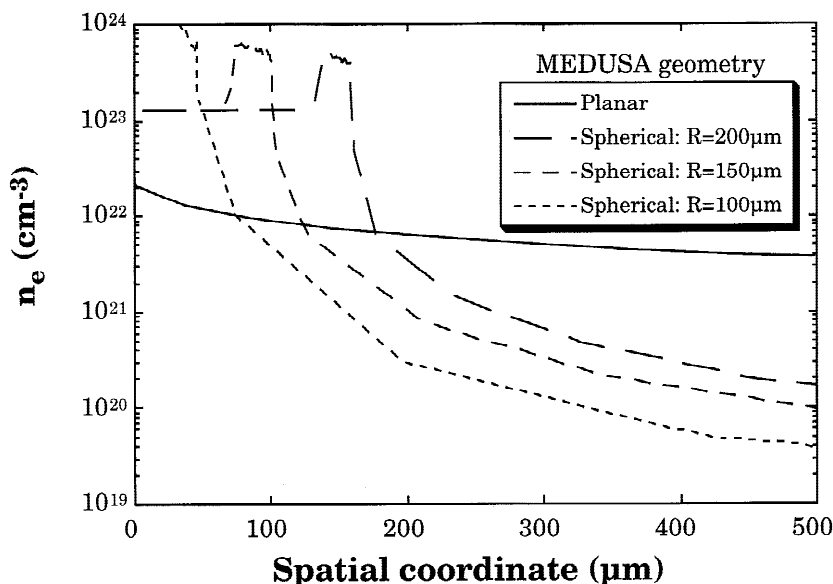


Fig. 7. Plasma electron density profiles at the peak of the laser pulse as simulated by MEDUSA in the standard planar geometry (continuous curve) and in the spherical geometry for three values of the target radius (dashed curves).

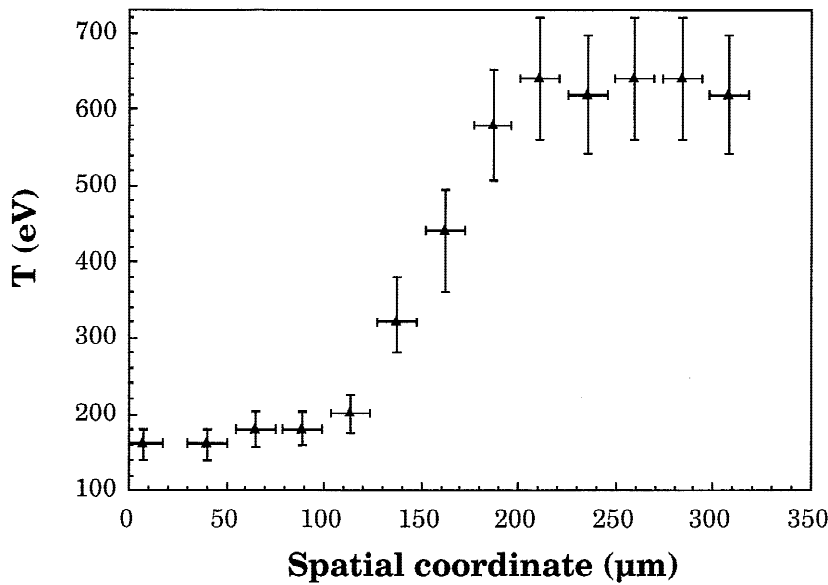


Fig. 8. Electron temperature profile of the plasma produced by the laser irradiation of a solid Al target by a nanosecond Nd laser. The spatially resolved measurement was carried out using a space-resolving X-ray crystal spectrometer equipped with a high-dynamic range-cooled CCD detector.

carry out the comparison of the $Ly\alpha$ to $He\beta$ intensity ratio with RATION simulations so as to complete the electron temperature profile in the intermediate region between $z \approx 75 \mu\text{m}$ and for $z \approx 200 \mu\text{m}$.

The final temperature profile is shown in Figure 8. According to the determination from the spatially integrated spectra, a plasma size ranging from 50 to 100 μm was used for the region around the critical surface, which is located at about 160 μm from the target. For regions closer to the original target position we took into account lower plasma sizes too. However, it is important to point out that in the marginal regions ($z \approx 100 \mu\text{m}$ and $z \approx 200 \mu\text{m}$), the uncertainties arising from plasma size determinations result in much lower errors than the experimental ones.

It is interesting to compare the electron temperature profile with an *integrated* temperature determination retrieved from spatially integrated spectra. By performing on these spectra an analysis similar to that described above, we were able to estimate an electron temperature of about 260 eV. Thus, according to Figure 8, the electron temperature in the overdense region is slightly lower than the temperature obtained by spatially integrated spectra. In contrast, the temperature rises to much greater values in the coronal region, where the strong laser energy deposition occurs. These results clearly show that space-resolved measurements are indeed necessary in the investigation of laser-produced plasma parameters and in particular in the case of plasma produced by laser interaction with solid targets where strong temperature/density gradients exist. Additional problems may arise from temporal integration (Duston *et al.*, 1983) which still exists in our measurements. However, previous experiments (Macchi *et al.*, 1996) have demonstrated that X-ray emission intensity closely follows the laser pulse intensity. Therefore we can consider the results of time-

integrated measurements as characteristic of the peak of the pulse, with time-smearing effects playing only a negligible effect.

4. SUMMARY AND CONCLUSIONS

The use of a space-resolving Bragg X-ray crystal spectrometer equipped with a 10- μm slit coupled to a high-dynamic range-cooled CCD camera allowed us to obtain X-ray spectra with high spatial resolution. This high spatial resolution was only possible thanks to the use of a high sensitivity, high-dynamic range-cooled CCD detector.

The spectra obtained in these conditions clearly show that large electron temperature and density differences exist in our plasmas over a longitudinal extent of 320 μm from the target surface. A temperature profile was obtained which shows that the electron temperature ranges from around 200 eV in the overdense region up to about 650 eV in the coronal region. These results have been compared with the results obtained from spatially integrated spectra which give an *integrated* temperature of approximately 260 eV.

Despite the small size of plasmas produced in our experimental conditions, our study clearly demonstrates the effectiveness of our space-resolved measurements in detecting large temperature and density gradients in a submillimeter scale plasma.

REFERENCES

- CHRISTIANSEN, J.P., ASHBY, D.E. & ROBERTS, K.V. (1974). *Comput. Phys. Commun.* **7**, 271.
 DUSTON, D., CLARK, R.W., DAVIS, J. & APRUZESE, J.P. (1983). *Phys. Rev. A* **27**, 1441.
 DUSTON, D. & DAVIS, J. (1980). *Phys. Rev. A* **21**, 1664.

- GIULIETTI, A., BENEDEUCE, C., CECCOTTI, T., GIULIETTI, D., GIZZI, L.A. & MILDREN, R. (1998). *Laser Part. Beams* **16**, 1.
- GIULIETTI, D. & GIZZI, L.A. (1998). *Riv. Nuovo Cimento* **21**, n.10.
- GIZZI, L.A., GIULIETTI, D., GIULIETTI, A., AFSHAR-RAD, T., BIANCALANA, V., CHESSA, P., DANSON, C., SCHIFANO, E., VIANA, S.M. & WILLI, O. (1994). *Phys. Rev. E* **49**, 5628.
- GRIEM, H.R. (1997). *Principles of Plasma Spectroscopy*. Cambridge University Press, UK.
- HAUER, A.A., DELAMATER, N.D. & KOENIG, Z.M. (1991). *Laser Part. Beams* **9**, 3.
- KAUFFMAN, R. (1991). In *Handbook of Plasma Physics* (Rubenchik, A., and Sagdeev, R.Z., Eds.), Vol. 3, p. 111. Amsterdam: North Holland.
- LEBOUCHER-DALIMIER, E., POQUÉRUSSE, A. & ANGELO, P. (1993). *Phys. Rev. E* **47**, 1467.
- LEE, R.W., WHITTEN, B.L. & STOUT II, R.E. (1984). *J. Quant. Spectrosc. Radiat. Transfer* **32**, 91.
- MACCHI, A., GIULIETTI, D., BASTIANI, S., GIULIETTI, A. & GIZZI, L.A. (1996). *Nuovo Cimento D* **18**, 727.
- MARZI, S., GIULIETTI, A., GIULIETTI, D., GIZZI, L.A. & SALVETTI, A. (2000). *Laser Part. Beams* **18**, 1.
- MAX C.E. (1982). In *Laser-Plasma Interaction, Proceedings of the Ecole d'été de physique théorique, Les Houches, session XXXIV* (Balian, R., and Adam, J.-C., Eds.), p. 301. Amsterdam: North-Holland.
- NANTEL, M., KLISNICK, A., JAMELOT, G., HOLDEN, P.B., RUS, B., CARILLON, A., JAÉGLÉ, P., ZEITOUN, PH., TALLENTS, G., MACPHEE, A.G., LEWIS, C.L.S., JACQUEMOT, S. & BONNET, L. (1996). *Phys. Rev. E* **54**, 2852.
- RODGERS, P.A., ROGOYSKI, A.M. & ROSE, S.J. (1989). *RAL Report* No. RAL-89-127 (unpublished).